

## The Orbit of the Near-Earth Asteroid 40329 (1999ML) 07/30/2016

Elisa Zhao Hang<sup>1</sup>, Hernan Valles<sup>1</sup>, Yiluo Li<sup>1</sup>  
<sup>1</sup>Summer Science Program at Colorado University, Boulder

### ABSTRACT

Considering the destructive impact brought by asteroids upon their collision with the Earth, it is crucial to study their orbits and predict, if any, the threat of collision in the future. With observational data collected from 16" telescope at Sommers-Bausch Observatory, this team was able to determine the orbit of the near-Earth asteroid 40329 (1999ML). The result deviated slightly from the previous orbital elements generated from the JPL Horizons System: the semi-major axis (**a**) was  $(2.28 \pm 0.20)$  AU; the eccentricity (**e**) was  $(0.456 \pm 0.043)$ ; the inclination (**i**) was  $(2.523 \pm 0.069)^\circ$ ; the longitude of ascending node ( **$\Omega$** ) was  $(211.8 \pm 5.6)^\circ$ ; the argument of perihelion ( **$\omega$** ) was  $(110.9 \pm 8.4)^\circ$ ; the mean anomaly (**M**) was  $(348.8 \pm 1.9)^\circ$ .

**Keyword:** Orbit Determination, Near-Earth Asteroid, Gaussian Methods

## I. INTRODUCTION

After Tunguska Event in 1908, the threats posed by near-Earth asteroids were brought to scientists' concern. Asteroids are destructive once entering the Earth's atmosphere. A Tunguska sized (estimated 40 meters across) asteroid could produce a fireball and release energy equivalent to about 185 Hiroshima Bombs [1]. If landed in a densely populated area, the asteroid could cause countless loss on the human side.

Therefore, the primary goal for this team during the Summer Science Program (SSP) was to determine the orbit of the near-Earth asteroid 40932 (1999ML). With 1999ML's orbital elements calculated, its orbit could be simulated to determine the possibility of collision in the future.

During SSP, 1999ML has a maximum altitude at roughly  $35^\circ$  and magnitude of around 16.3 at night; therefore, this team was able to take usable images for 1999ML with the 16" telescope at Sommers-Bausch Observatory while successfully identify the asteroid position for further calculations.

## II. METHOD

### DATA COLLECTION

To identify the star field where 1999ML located in the night sky, this team relied initially on the ephemeris generator of the JPL Horizon System to obtain basic information of 1999ML (right ascension, declination, altitude, azimuth, apparent magnitude, and hour angle). With this information ready, a sky chart was generated using the system from the United States Naval Observatory (USNO). This sky chart would be used to match the star field from the images taken. Prior to the observation, the weather condition was consulted from the Clear Sky Chart website to make sure good conditions for the actual observation.

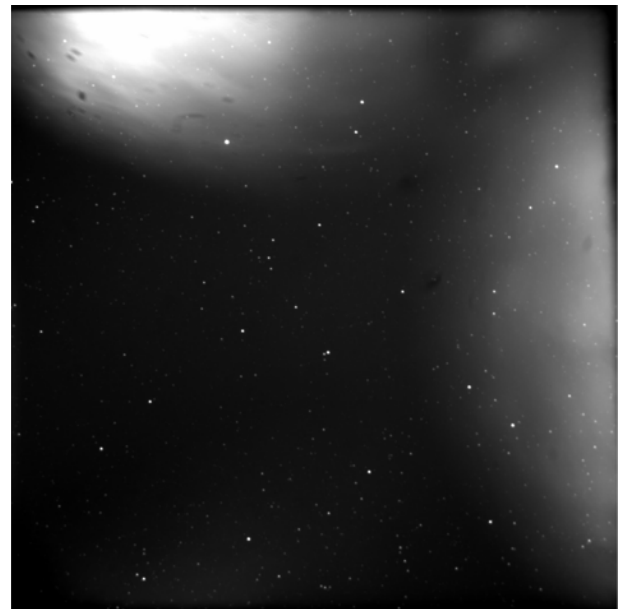


FIG. 1. Bad observation results with large patches of noises when pointing at low altitude celestial objects.

During the observation session, if the telescope was slewed directly to the asteroid position, it was possible that it would become less accurate due to the movement of the telescope. 1999ML was a rather faint and small object in the night sky; therefore once the inaccuracy built up, 1999ML could be missing from the image or become harder to spot in the images taken. To minimize this error, telescope was first pointed at Vega since it was near the zenith during the observation session; since the telescope was always pointed at zenith at initialization, the slewing distance between Vega and zenith was rather small.

When the telescope was pointed at Vega, a 1-second exposure was taken for it. From the image, this team was able to determine how much the star was off from the center (where it should appear in the image). After this, the

exposure mode was switched to continuous 1-second exposures, and by manually adjusting the pointing direction of the telescope, the star appeared at the center of the image. At this point, the telescope pointing direction could be initialized so the system could correct for the error generated from the movement.

After Vega, this team identified the rough position of 1999ML on the built-in sky chart in the computer and slewed the telescope to the star closest to 1999ML (normally it was between Sct-Alpha and Sct-Gamma depending on the position of the asteroid). The same calibration process for Vega was repeated on this star.

When the star appeared centered on the image, the calibration for focusing was carried out manually. Under continuous 1-second exposures, this team took subframes on one rather faint star on the image because it was crucial that a faint object like 1999ML could be spot clearly on the image. When the Point Spread Function showed an apparent peak, the calibration was considered successful, and the telescope could be slewed to 1999ML by inputting the right ascension and declination generated from the JPL Horizon System.

One exposure of 20 - 30 seconds was taken to get a clear view of the star field. The image was compared with the sky chart obtained from the USNO. Rotation of the sky chart was necessary when matching the stars. It was just a final check whether 1999ML was in the frame. Once the sky chart matched the image taken, three sets of five images were taken, each with a 180-second exposure time. Between each two sets, there would be a gap of roughly 6 - 8 minutes to ensure that the asteroid moved on the image. After taking the images, each set was aligned based on star patterns and was stacked. The three stacked images from the three would be aligned as well based on star patterns. After this process, the three stacked images were animated to search for 1999ML. It appeared as a faint dot that was apparently moving on the image.

## TECHNICAL PROBLEMS

At the beginning of SSP, the observations of this team were constantly canceled due to bad weather condition.

However, after the sky was cleared, the CCD did not appear to function well. Huge patches of noises and white dots were appearing on the images. While taking images of bright stars like Vega, it could be identified from the images. This problem was reported and soon fixed. It was due to the looseness of the CCD camera.

There was another problem in the following observation: the noises were reduced and Vega was identifiable, but when the telescope was pointing at a low altitude object (direction of 1999ML), the same pattern of white patches started to appear. By examining the pattern of the noises (corresponding to the directions of the door and computers) as shown in **Figure 1**, this team hypothesized that there was a light leak of the CCD camera.

When the telescope was pointed upward (at Vega), the CCD camera was facing downward at the floor, which was not directing facing the light sources. Therefore, this team

tested the hypothesis by holding up a black jacket as cover around the CCD when it was taking exposure of 1999ML. The major noises patches were largely removed from the resulting images. While taking long exposures for consecutive images, the light sources were therefore covered up to decrease the level of light leak. This problem was also reported and found out to be caused by a missing screw, which left a hole opened for light to enter in the CCD camera.

The image quality was increased, but the asteroid was not identifiable. When this team was checking the match with the sky chart, it could not be matched, which was later found out to be a problem of ephemeris generation. The wrong coordinate system (apparent right ascension and declination) was used to generate information about 1999ML. It should be astronomic right ascension and declination (J2000).

## CENTROID AND LSPR

First step of data processing was to obtain the right ascension and calculation though the images taken.

To get more accurate x and y coordinate of any objects from an image, a process of determining the centroid was required. It was a process similar to the determination of center of mass. Using Equation (1) and Equation (2), this team was able to obtain actual center of the object on the image starting from a rough guess.

$$x_{centroid} = \sum_{i=0}^n x_i p \quad (1)$$

Equation (1) calculates the x coordinate of the centroid, in which  $x_i$  represents the horizontal distance of the pixel from the center of initial guess, and  $p$  represents the pixel count of that particular pixel.

$$y_{centroid} = \sum_{i=0}^n y_i p \quad (2)$$

Equation (2) calculates the y coordinate of the centroid, in which  $y_i$  represents the vertical distance of the pixel from the center of initial guess.

After the centroid of 1999ML was calculated, reference stars were necessary for the calculation of right ascension and declination of 1999ML. By using the ESO-DSS I/II image server with initial right ascension and declination obtained from the JPL Horizon, a star field that matched 1999ML's image was generated, where six bright stars were chosen around 1999ML. The stars information in the image serve contained their right ascension and declination. These stars were easily identifiable from the image taken for 1999ML; therefore the x and y coordinates for the reference stars could be found on the image taken for 1999ML. These values were initial guesses that were sufficient enough to pass on to the centroid equations, where more accurate x and y coordinates could be determined.

With right ascension, declination, and x and y coordinates of the reference stars, Least Squared Plate Reduction method was applied to find the plate coefficient of the image, which could then be passed on to Equation (3) and (4) to find the right ascension and declination of 1999ML given the x and y coordinate of it:

$$\alpha = b_1 + a_{11}x + a_{12}y \quad (3)$$

$$\delta = b_2 + a_{21}x + a_{22}y \quad (4)$$

Equation (3) and (4). These are equations used to find right ascension ( $\alpha$ ) and declination ( $\delta$ ) of the objects with known x and y coordinates in the image with known plate coefficients ( $b_1, b_2, a_{11}, a_{12}, a_{21}, a_{22}$ ).

ORBITAL ELEMENTS

With calculations of right ascension and declination for three observations ready, the unit vectors of all three asteroid position vectors ( $\rho_{-1}, \rho_0, \rho_{+1}$  as indicated in **Figure 2**) were calculated.

To proceed with the calculation with rather convenient mathematical process, time was converted from Julian Dates to Gaussian Days ( $\tau$ ):

$$\tau_{-1} = k(t_{-1} - t_0) \quad (5)$$

$$\tau_0 = k(t_{+1} - t_{-1}) \quad (6)$$

$$\tau_{+1} = k(t_{+1} - t_0) \quad (7)$$

Equation (5), (6), and (7) convert time from Julian Dates to  $\tau$ , in which  $k$  is the Gaussian Constant, and  $t_{-1}, t_0, t_{+1}$  are time of observations in Julian Dates.

With two vectors of different and non-parallel directions, a third vector could be obtained by linear combination:

$$r_0 = a_{-1}r_{-1} + a_{+1}r_{+1} \quad (8)$$

Equation (8) explained the the linear combination of the three asteroid position vectors ( $r_{-1}, r_0, r_{+1}$ ) and  $a_{-1}$  and  $a_{+1}$  are scalars to be determined.

The scalars  $a_{-1}$  and  $a_{+1}$  were calculated from the  $\tau$  values, and the magnitude of  $\rho_{-1}, \rho_0$ , and  $\rho_{+1}$  could then be found with scalars  $a_{-1}$  and  $a_{+1}$ .

Then the position ( $r_0$ ) and velocity ( $v_0$ ) vectors originated from the Sun could be calculated through the values obtained so far.

As illustrated in **Figure 3**, an iteration was carried out by using another method to calculated the scalars  $a_{-1}$  and  $a_{+1}$ . Then the iteration continued until the difference between calculated magnitude value for  $r_0$  vector and previously calculated magnitude value for  $r_0$  vector was smaller than  $10^{-9}$ .

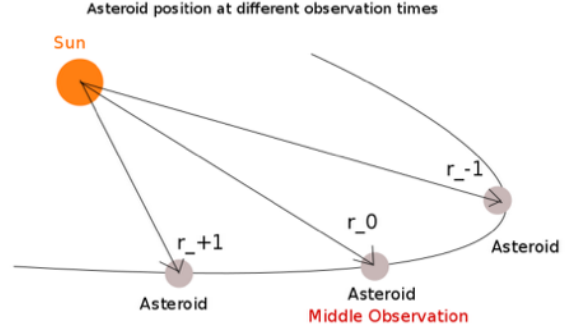


FIG. 2. Visual representation of asteroid position vectors originated from the Sun.

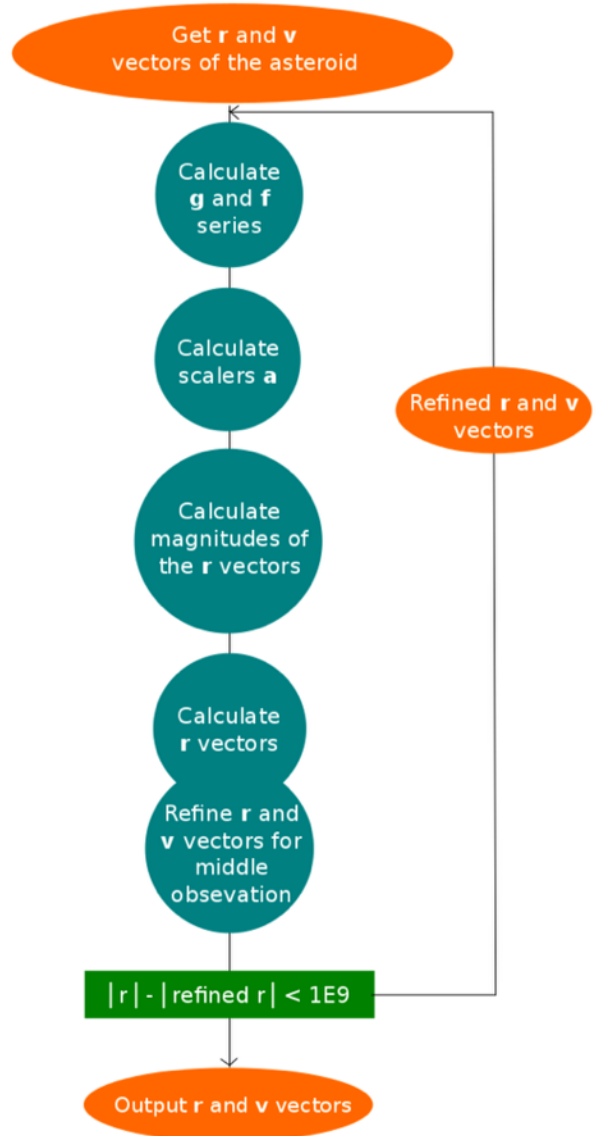


FIG. 3. Flow chart of the algorithm used to calculate  $r$  and  $v$  vectors of the asteroid as seen from the Earth.

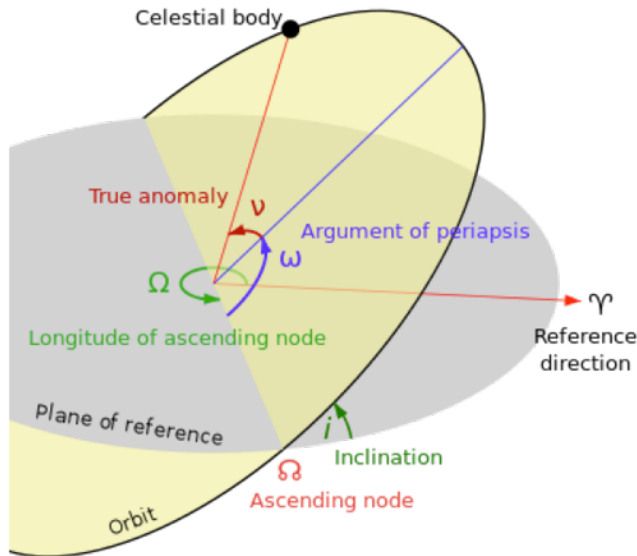


FIG. 4. Illustration of Orbital Elements [2]

During the iteration,  $\mathbf{v}_0$  vector was also updated; therefore, when the  $\mathbf{r}_0$  vector was obtained,  $\mathbf{v}_0$  vector was updated as well.

Using Vis-Viva equation, a vector perpendicular to the asteroid plane was calculated for further calculation. By order, semi-major axis, eccentricity, inclination, longitude of ascending node, argument of perihelion, and mean anomaly (as illustrated in **Figure 4**) could be obtained from  $\mathbf{r}_0$  vector and  $\mathbf{v}_0$  vector.

### III. RESULTS

**Table 1** shows the right ascension, declination, and magnitude calculated through the centroid and LSPR methods. These values were then used to calculate the orbital elements of asteroid 1999ML.

**Table 2** shows the calculated orbital elements from the asteroid image sets. Although only four sets of pictures were collected directly by this group, four more sets from another research group were included to allow an increase in the number of combinations of image sets.

These combinations allow calculations of orbital elements with data that has different time spacing, which results in a wider spread of results that can then be median and mean combined to achieve more accurate orbital element calculations.

The relatively small standard deviation reveals that there is very little random error in the calculated orbital elements.

#### CCD IMAGES OF ASTEROID

The images with circled stars were obtained from the image server ESO-DSS I/II and the PPMX catalog. The reference stars used to calculate the magnitude of the asteroid are numbered and circled in red. The asteroid itself is circled in green.

The inverted color images are the images taken by this research team. They can be matched with the images generated from the server in order to locate the reference stars.

#### Results of observation for Asteroid 1999ML

Time of Observation		Right Ascension		Declination		Magnitude Estimate	Signal to Noise Ratio
MM/DD/UT	Julian Days	HH MM SS	Decimal	DD MM SS	Decimal		
07/08/08:33:53	2457577.85687	18 42 22.706	18.706307	-12 44 27.23	-12.74089	16.8	58.24
07/12/07:50:14	2457581.82655	18 43 9.525	18.719312	-12 17 25.05	-12.29029	16.7	45.975
07/15/08:47:06	2457584.86604	18 44 1.199	18.733666	-11 58 35.90	-11.97664	16.1	43.195
07/24/07:47:38	2457593.82475	18 48 32.526	18.809035	-11 14 30.48	-11.2418	16.1	51.84

TAB 1. Right ascension, declination, magnitude and signal to noise ratio as calculated from four observations

**Orbital Elements and Uncertainties**

	Image Sets Used					Mean	Median	Standard Deviation
	8, 12, 14	8, 12, 15	8, 14, 24	8, 15, 23	24, 26, 28			
$\vec{r}$	0.406067	0.409378	0.437013	0.453321	0.621315	0.465419	0.437013	0.089331
	-1.166939	-1.184311	-1.149287	-1.141072	-1.049808	-1.138283	-1.149287	0.052193
	-0.4441	-0.448030	-0.436802	-0.433128	-0.391742	-0.430776	-0.436802	0.022599
$\vec{v}$	0.913282	0.913849	0.906569	0.903263	0.843346	0.896062	0.906569	0.029808
	0.458396	0.460682	0.476946	0.484312	0.645197	0.505107	0.476946	0.079066
	0.201199	0.203718	0.207953	0.211105	0.260999	0.216995	0.207953	0.024893
a	2.280226	2.415141	2.271933	2.266966	2.737107	2.394275	2.280226	0.201340
e	0.456182	0.479773	0.455125	0.453296	0.553880	0.479651	0.456182	0.042886
i	2.522593	2.659181	2.508236	2.515041	2.615302	2.564071	2.522593	0.068761
$\Omega$	211.8133	213.4453	211.4747	211.8956	199.7585	209.6775	211.8133	5.5967
$\omega$	110.8831	108.6409	111.4018	110.7523	129.0154	114.1387	110.8831	8.3830
M	348.0295	349.0528	348.5014	348.8227	352.6556	349.4124	348.8227	1.8532

TAB 2. Calculated orbital elements from five observations. Each calculation requires three sets of images. The numbers under image sets used represent the three dates in July, 2016 on which the images were taken.

07/12/2016 07:50:14 UTC

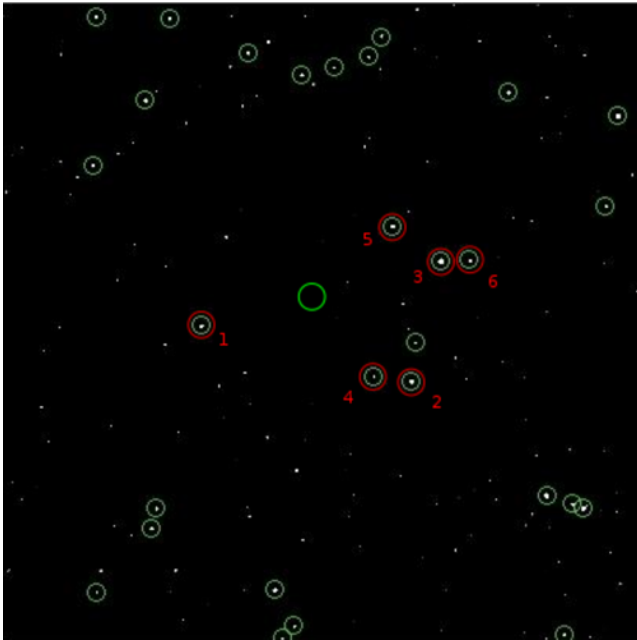


FIG. 5a. Stars within red circles are reference stars. Green circle represents the field where the asteroid locates.

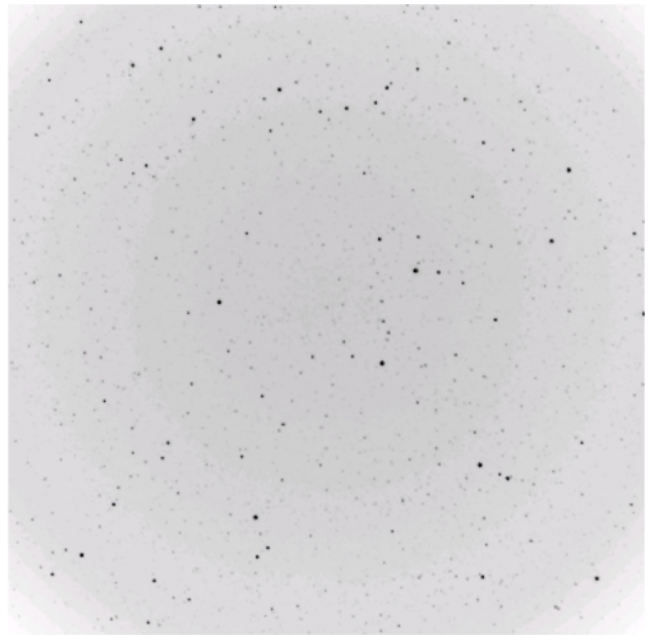


FIG.5b. The negative image of **Figure 5a**

07/12/2016 07:50:14 UTC

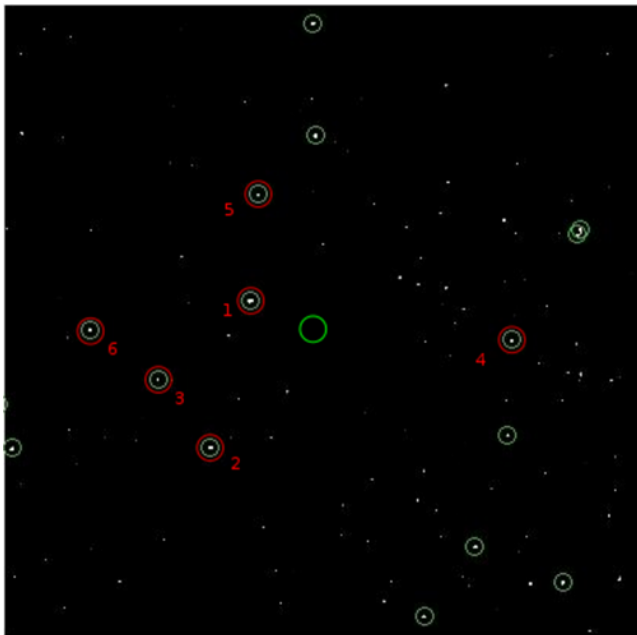


FIG. 6a

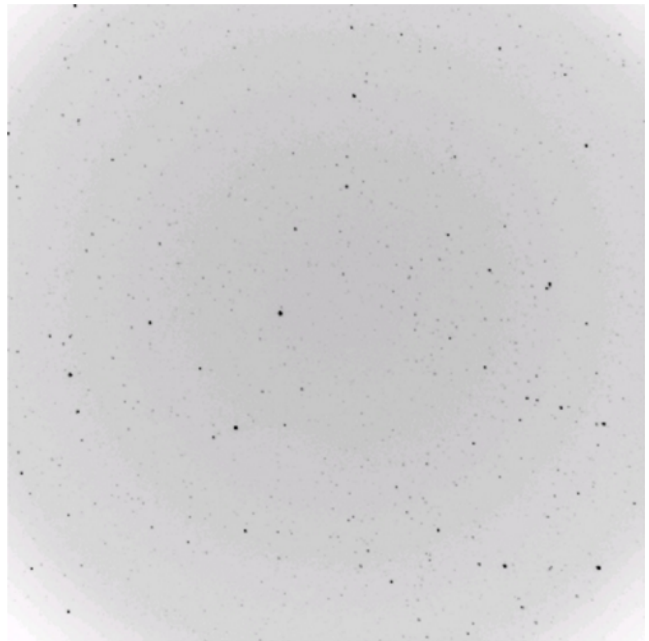


FIG.6b. The negative image of **Figure 6a**

07/15/2016 08:47:06 UTC

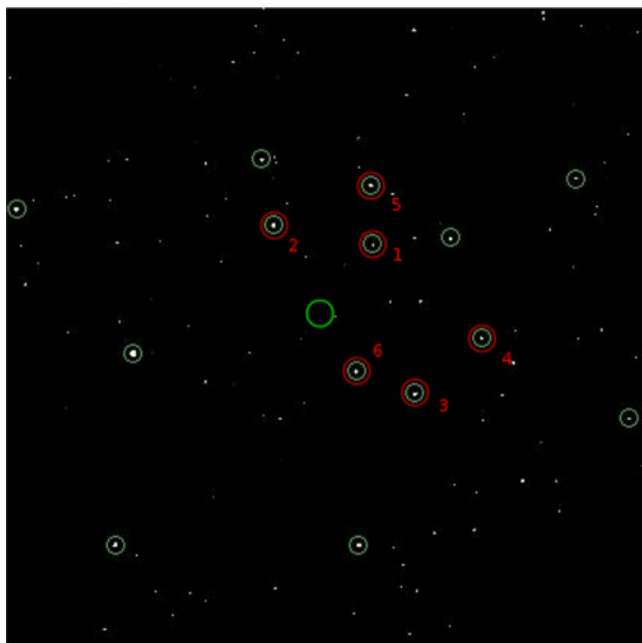


FIG.7a

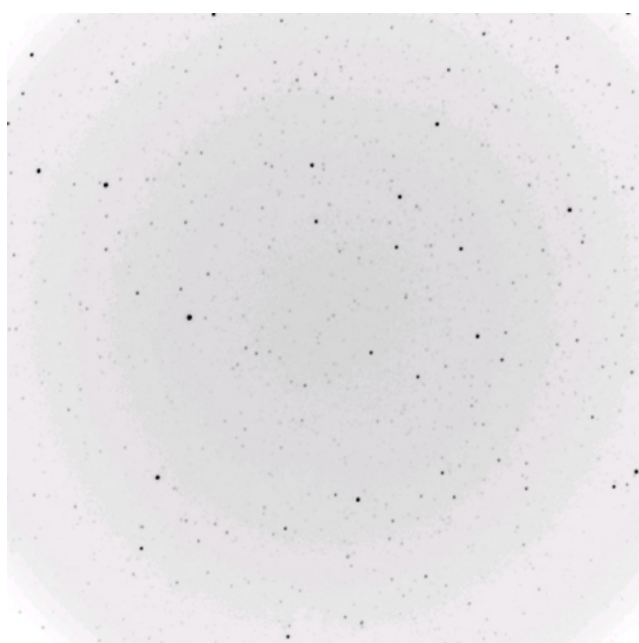


FIG.7b. The negative image of **Figure 7a**

07/24/07:47:38 UTC

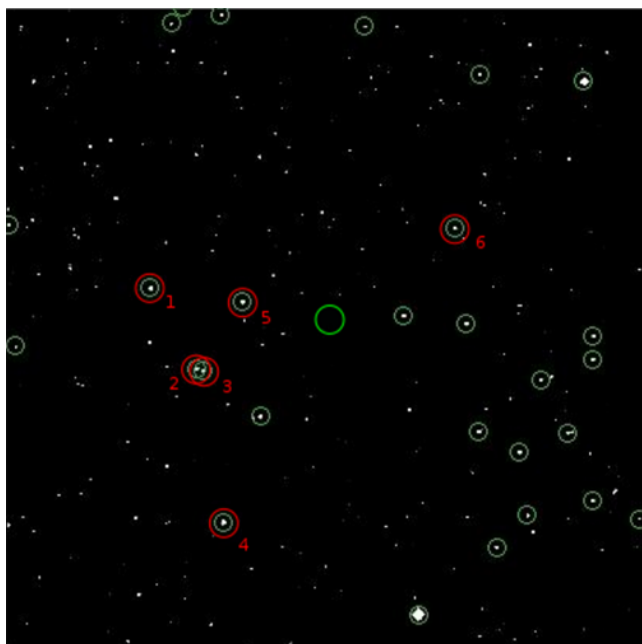


Fig. 8a



FIG.8b. The negative image of **Figure 8a**

### Orbital Elements from JPL Horizons VS. Calculated Values (Julian Dates: 2457581.82655)

Orbital Elements	JPL Values [3]	Calculated Values	Percent Error (%)
Semi-major axis (a)	2.26572 (AU)	2.280226 (AU)	0.64
Eccentricity (e)	0.454234	0.456182	0.43
Inclination (i)	2.52085°	2.52259°	0.00048
Longitude of ascending node ( $\Omega$ )	210.974°	211.813°	0.23
Argument of perihelion( $\omega$ )	112.014°	110.883°	0.31
Mean anomaly (M)	347.855°	348.823	0.27

TAB 3. Comparison of JPL values and computed values for orbital elements

Table 3 displays the difference between the JPL Horizons values and the computed values for the orbital elements. The calculated values included were the median-combined values from Table 2, as some of set combinations - such as the set that combined images from July 24, 26 and 28 - yielded orbital elements that were noticeably different from most of the other set combinations.

The low percentage error for the calculated values suggests that the computation of orbital elements from the asteroid images was significantly close to the expected values obtained from JPL Horizons. As some of the error can be accounted for by the uneven spacing of some observations, it can be concluded that the orbital elements calculated are fairly accurate.

#### IV. CONCLUSION

Through the calculations of the orbital elements, it is possible to conclude that the orbit of asteroid 40392 (1999ML) has not changed significantly since data was collected by JPL Horizons.

This research revealed that Gauss' method is somewhat affected by the uneven spacing of observations, however there does not seem to be a very significant effect.

After visualizing the orbit of the asteroid, as shown in Figure 8, it has been determined that the orbit of asteroid 1999ML does not intersect with the orbit of Earth.

Therefore, the probability for the asteroid to hit the Earth is not very high. Although, because the orbit of the asteroid crosses the orbit of Mars, there is a possibility that after thousands of years, a near collision with Mars will either destroy the asteroid or change its orbit due to their close proximity, potentially causing the asteroid's trajectory to change into a hyperbolic trajectory.

More data is needed to determine when and if the asteroid will collide with Mars.

#### V. REFERENCE

- [1] T. Phillips, "The Tunguska Impact--100 Years Later - NASA Science", Science.nasa.gov, 2016. [Online]. Available: [http://science.nasa.gov/science-news/science-at-nasa/2008/30jun\\_tunguska/](http://science.nasa.gov/science-news/science-at-nasa/2008/30jun_tunguska/). [Accessed: 30- Jul- 2016].
- [2] P. E. Hardy. Orbital Maneuver Applications & Capabilities of the ALL-STAR CubeSat Propulsion System. [Online]. Available: [http://ccar.colorado.edu/asen5050/projects/projects\\_2013/Hardy\\_Paul](http://ccar.colorado.edu/asen5050/projects/projects_2013/Hardy_Paul)
- [3] "HORIZONS System", Ssd.jpl.nasa.gov, 2016. [Online]. Available: <http://ssd.jpl.nasa.gov/?horizons>. [Accessed: 30- Jul- 2016].

#### VI. ACKNOWLEDGEMENT

We would like to acknowledge Summer Science Program and Sommers-Bausch Observatory at Colorado University, Boulder for allowing us access to the telescope and the opportunity to study Near-Earth Asteroids.

Secondly, we would like to acknowledge Dr. Michael Dubson as Academic Director of this program, Dr. Cassandra Fallscheer as Associate Academic Director, and Ms. Barbara Martinez as Site Director.

We would also like to acknowledge Ioana Plesca, Isabella Sanders, Andrew Bundas, and Sam Holos as our kind and often patient Teaching Assistants and Residential Mentors.

Finally, we would like to acknowledge Team 5 of SSP of providing us extra observation data to increase our accuracy.

## VII.

## APPENDIX

## APPENDIX I

## Results of Observation for Asteroid 1999ML

Time of observation		Right Ascension		Declination		Magnitude Estimate	Signal to Noise Ratio
MM/DD/UT	Julian Days	HH MM SS	Decimal	DD MM SS	Decimal		
07/08/08:33: 53	2457577.85687	18, 42, 22.706	18.70631	-12, 44, 27.23	-12.74089	16.8	58.24
07/12/07:50: 14	2457581.82655	18, 43, 9.525	18.719312	-12, 17, 25.05	-12.29029	16.7	45.98
07/15/08:47: 06	2457584.86604	18, 44, 1.199	18.733666	-11, 58, 35.90	-11.97664	16.1	43.20
07/24/07:47: 38	2457593.82475	18, 48, 32.526	18.809035	-11, 14, 30.48	-11.2418	16.1	51.84

## APPENDIX II

Summary Table of Iterations of  $\mathbf{r}$  and  $\mathbf{v}$  Vectors

Iteration #	$\mathbf{r}$ vector	$\mathbf{v}$ vector
Initial Guess	-12.3027777214 65.2340329312 14.276785175	-16.9726703354 73.1326547555 8.86779286
1	0.467113015275 -1.44805296786 -0.50675478835	0.900882348917 0.595350317334 0.26617527293
2	0.229788035516 -0.168176665134 -0.22961841651	0.898330293058 0.070783497152 0.03905010191
3	-2.14752997988 12.2259978155 2.5339658938	1.18360519353 -5.26824118323 -2.6162913967
4	0.465505485001 -1.44311252853 -0.50506061221	0.90463971752 0.584858487028 0.26251192891
5	0.435430917943 -1.28563790349 -0.4700648246	0.911561491074 0.499418050062 0.22506187909
6	0.427675657901 -1.24501680502 -0.46104559795	0.911741089002 0.485238951278 0.21727593782
7	0.424170850758 -1.22665386687 -0.45696770936	0.912325755647 0.476186723734 0.21316411461
8	0.42245254545 -1.21765054858 -0.45496844996	0.912604096323 0.471789310142 0.21115792781
9	0.421574814093 -1.21305139684 -0.4539471967	0.912746880575 0.469539466472 0.21013242494
10	0.421117357222 -1.21065436793 -0.45341493795	0.912821200509 0.468367275758 0.20959806422
11	0.420876445999 -1.2093920061 -0.45313463339	0.912860319625 0.467750035422 0.20931667620
12	0.42074888106 -1.20872356966 -0.45298620919	0.912881027583 0.467423222578 0.2091676853
13	0.420681139321 -1.20836860414 -0.45290739038	0.912892022615 0.467249678868 0.20908856754
14	0.420645110943 -1.20817981583 -0.45286547067	0.912897869842 0.467157381529 0.2090464893

15	0.420625933723 -1.20807932734 -0.45284315760	0.912900982077 0.467108253894 0.20902409211
16	0.420615721643 -1.20802581609 -0.45283127565	0.912902639339 0.467082093027 0.20901216536
17	0.420610282348 -1.20799731421 -0.45282494692	0.912903522042 0.467068158913 0.20900581279
18	0.420607384842 -1.20798213129 -0.45282157562	0.912903992253 0.46706073624 0.20900242879
19	0.420605841244 -1.20797404284 -0.45281977961	0.91290424275 0.467056781937 0.20900062602
20	0.420605018889 -1.20796973371 -0.45281882278	0.912904376202 0.467054675275 0.20899966559
21	0.42060458077 -1.20796743796 -0.45281831302	0.9129044473 0.467053552926 0.20899915391
22	0.420604347354 -1.20796621487 -0.45281804144	0.912904485179 0.467052954976 0.20899888131
23	0.420604222998 -1.20796556324 -0.45281789675	0.91290450536 0.467052636406 0.20899873607
24	0.420604156744 -1.20796521607 -0.45281781966	0.912904516111 0.467052466681 0.20899865869
25	0.420604121446 -1.2079650311 -0.45281777859	0.912904521839 0.467052376256 0.20899861747
26	0.42060410264 -1.20796493256 -0.45281775671	0.912904524891 0.46705232808 0.2089985955
27	0.420604092621 -1.20796488006 -0.45281774505	0.912904526517 0.467052302413 0.20899858380
28	0.420604087283 -1.20796485209 -0.45281773884	0.912904527384 0.467052288739 0.20899857757
29	0.420604084439 -1.20796483719 -0.45281773553	0.912904527845 0.467052281453 0.20899857425
30	0.420604082924 -1.20796482925 -0.45281773377	0.912904528091 0.467052277572 0.20899857248
31	0.420604082116 -1.20796482502 -0.45281773283	0.912904528222 0.467052275504 0.20899857154
32	0.420604081686 -1.20796482276 -0.45281773233	0.912904528292 0.467052274402 0.20899857103
33	0.420604081457 -1.20796482156 -0.45281773206	0.912904528329 0.467052273816 0.20899857077
34	0.420604081335 -1.20796482092 -0.452817731926	0.912904528349 0.467052273503 0.20899857062

## APPENDIX III

**Uncertainty of Calculated Orbital Elements**

Quantity	Value	Uncertainty
Semi-major Axis (a)	2.280226 (AU)	$\pm 0.64$ (AU)
Eccentricity (e)	0.456182	$\pm 0.43$
Inclination (i)	2.522593°	$\pm 0.00048^\circ$
Longitude of Ascending Node ( $\Omega$ )	211.8133°	$\pm 0.23^\circ$
Argument of Perihelion ( $\omega$ )	110.8831°	$\pm 0.31^\circ$
Mean Anomaly (M)	348.8227°	$\pm 0.27^\circ$